Endogenous Buffers Limit the Spread of Free Calcium in Hair Cells

Jon D. Hall, Sandeep Betarbet, and Fernán Jaramillo
Department of Physiology, Emory University School of Medicine, Atlanta, Georgia 30322 USA

ABSTRACT Mobile Ca^{2+} buffers in hair cells have been postulated to play a dual role. On one hand, they carry incoming Ca^{2+} away from synaptic areas, allowing synapses to be rapidly reset. On the other hand, they limit the spread of free Ca^{2+} into the cell, preventing cross-talk between different pathways that employ Ca^{2+} as a second messenger. We have obtained evidence for such mobile Ca^{2+} buffers in hair cells by comparing the patterns of Ca^{2+}-induced fluo-3 fluorescence under whole-cell and perforated-patch recording conditions. Fluorescent signals under perforated-patch conditions are relatively weak and are limited to the immediate vicinity of the membrane. These observations can be explained by a diffusion-reaction scheme that, in addition to Ca^{2+} and fluo-3, incorporates endogenous fixed and mobile Ca^{2+} buffers. Our experiments also suggest that the mobility of the endogenous buffer might be higher than previously thought. A high buffer mobility is expected to enhance the cell's ability to rapidly modulate transmitter release.

INTRODUCTION

The hair cell's afferent synapse is particularly interesting because of its extraordinary capacity for precise relaying of timing and intensity information. This ability depends largely on the mechanisms employed by the hair cell for rapidly modifying the Ca^{2+} concentration in the vicinity of transmitter release sites. Increases in Ca^{2+} concentration are brought about by the receptor potential-induced opening of voltage-dependent Ca^{2+} channels that are localized to synaptic "active zones." A number of mechanisms are used by the hair cell for decreasing Ca^{2+} concentration. Among these are simple diffusion of Ca^{2+} away from its site of action, Ca^{2+} buffering, and active extrusion (Roberts, 1994). If we are to understand how hair cell synapses accomplish their task, it is necessary to describe the dynamics of Ca^{2+} near transmitter release sites.

Past attempts at understanding Ca^{2+} dynamics in hair cells have followed either experimental or theoretical lines. Experimental approaches typically combine Ca^{2+}-sensitive fluorescent indicators and confocal microscopy to produce images of the patterns of fluorescence of a Ca·indicator complex following various stimulation protocols (Issa and Hudspeth, 1994, 1996b; Tucker and Fettiplace, 1995). Unfortunately, such optical methods do not offer sufficient spatial resolution. Theoretical approaches involve mathematical modeling of the classical diffusion-reaction scheme, where Ca^{2+} entering the cell binds to one or more species (Roberts, 1994; Wu et al., 1996). It must be emphasized that theoretical and experimental approaches are not necessarily divorced. The mathematical modeling of Ca^{2+} dynamics in the vicinity of active zones (Roberts, 1994) follows earlier work that described the role of endogenous Ca^{2+} buffers in regulating the activity of Ca^{2+}-activated potassium channels (Roberts, 1993). Comparable modeling techniques have also been used by Issa and Hudspeth to explain the patterns of Ca^{2+}-induced fluo-3 fluorescence in hair cells. However, the value of these models has been limited by the general lack of information regarding certain parameter values, such as the diffusion coefficients of Ca^{2+} indicators and Ca^{2+}-binding proteins in hair cells, as well as their affinities for different ions. Furthermore, these models have not provided a detailed account of experimentally obtained data, and therefore they remain largely untested.

We have attempted to produce a more thorough understanding of Ca^{2+} dynamics by combining these two methods, in an effort to reduce the potential error of either single method. Using experimentally determined values for most parameters, we have developed a useful theoretical model. We have tested the accuracy of the model by comparing theoretical results with experimentally obtained confocal images of hair cells voltage-clamped by either whole-cell or perforated-patch methods. Our results suggest that the patterns of fluorescence observed under whole-cell recording conditions cannot be fully explained by a simple diffusion-reaction scheme involving Ca^{2+} and a Ca^{2+} indicator (Issa and Hudspeth, 1996b). Finally, based on our confidence in the accuracy of the model to predict the main features of Ca·indicator complex fluorescence patterns, we have modeled the Ca^{2+} concentration in the immediate vicinity of the release sites. Our results confirm the important role endogenous buffers play in modifying the concentration of Ca^{2+} near the transmitter release sites of hair cells, as well as in determining the extent to which free Ca^{2+} spreads into the cell.

Received for publication 9 May 1997 and in final form 10 June 1997.

Address reprint requests to Fernán Jaramillo, Department of Physiology, Emory University School of Medicine, 255 Physiology Bldg., 1648 Pierce Drive, Atlanta, GA 30322. Tel.: 404-727-9675; Fax: 404-727-2648; E-mail: fjaram@physio.emory.edu.

Part of this work has previously been published in abstract form (Jaramillo et al., 1996).

0006-3495/97/09/1243/10 $2.00

MATERIALS AND METHODS

Electrophysiology

Hair cells were obtained from the maculae sacculi of leopard frogs (*Rana pipiens*) following previously published methods (Assad et al., 1989; Issa

and Hudspeth, 1994). All electrophysiology experiments were conducted at room temperature (20–25°C) in normal-Ca^{2+} saline (NCS) (mM: 110 NaCl, 2 KCl, 4 $CaCl_2$, 3 glucose, 5 HEPES, pH 7.25, with 1 N NaOH).

For conventional whole-cell recording, electrodes (3–5 MΩ) were tip-filled with a solution consisting of (mM) 102 CsCl, 2 NaCl, 1 ATP·2 Mg, 5 HEPES, and 0.1 fluo-3, pentapotassium salt (Molecular Probes, Eugene, OR) (pH 7.3 with CsOH) and then back-filled with the same solution minus fluo-3. Divalent cations were removed from the internal solution by incubation with Chelex 100 chelating resin (Sigma, St. Louis, MO). The concentration of Ca^{2+} in these solutions was estimated below 10^{-9} M by the use of calcium-sensitive electrodes that were calibrated against Ca^{2+} standards (Calbuf-1; WPI, Sarasota, FL) at the time of use. Ca^{2+}-sensitive electrodes were made using the highly selective Ca^{2+} ionophore II (Fluka, Ronkonkoma, NY) (Schefer et al., 1986). Electrodes exhibited near-Nernstian behavior down to 10^{-8} M free Ca^{2+}. A free Ca^{2+} concentration below 10^{-9} M in the internal solution was inferred on the basis of a $>$ −30-mV electrode shift upon transferring into internal solution from a 10^{-8} M free Ca^{2+} solution. For perforated-patch recordings, cells were loaded with the acetoxymethyl (AM) ester form of fluo-3 (Molecular Probes), according to the manufacturer's instructions. Electrodes were filled with a solution consisting of (mM) 102 Cs-aspartate, 2 NaCl, and 5 HEPES (pH 7.3 with CsOH). In addition, the electrode filling solution contained nystatin (Sigma) to a final concentration of 150 μg/ml. Voltage clamp was performed using either an APC-8 Amplifier (Medical Systems, Greenvale, NY) or an Axopatch 200B Amplifier (Axon Instruments, Foster City, CA). Whole-cell currents were filtered at 5 kHz (−3 db, 4-pole Bessel) and sampled at 10 kHz before being stored to disk.

Calbindin-D9k (Sigma) was labeled with fluorescein isothiocyanate (FITC) (Molecular Probes), according to the manufacturer's instructions. Labeled protein was separated from free dye on a Sephadex G-25 column. The labeled fraction was dialyzed for 24 h with a 10-kDa cutoff membrane, with no loss of fluorescence, indicating that the dye was coupled to a complex of at least this size (it is worth noting that the molecular mass of calbindin-D9k, estimated by gel filtration, is 11 kDa). Based on the fraction of the dye retained in the column, we estimate that two or three FITC molecules were incorporated for every molecule of calbindin-D9k.

Confocal microscopy

Confocal microscopy was performed with a Bio-Rad MRC600 equipped with a krypton/argon laser (model 5470K; Ion Laser Technology, Salt Lake City, UT) and a standard FITC filter package. The MRC600 was coupled to an Axiovert 135 inverted microscope (Carl Zeiss, Oberkochen, Germany) equipped with a 63×, 1.4 NA oil objective. Optical zoom was set to conform with the Nyquist criterion for spatial sampling. Lateral and axial resolution were estimated by three-dimensional confocal scanning of 100-nm fluorescent beads. Their lateral fluorescence (x,y plane) and optical axis (z direction) fluorescence patterns were well fitted by Gaussian curves with $\sigma = 0.25$ μm and 0.7 μm, respectively (image analysis was performed with National Institutes of Health Image 1.60). These Gaussian curves were used as an empirical estimate of the confocal microscope point spread function.

Hair cell images (e.g., Fig. 2 *A*) are composed of 512 2-ms scans, with individual scans sweeping from bottom to top, and consecutive scans advancing from left to right. Typically, cells were oriented "horizontally"; thus successive scans advanced from the hair bundle toward the basal pole. About 1 s is required to acquire the entire image. A 150-ms depolarizing pulse delivered while a cell was being scanned is represented by a 75-pixel horizontal bar, the position of which coincides with the period during which the cell was stimulated.

A number of measures were taken to attain a better understanding of the dynamics of Ca^{2+} near the cell's membrane. We sought active zones in which the dense bodies were not stained, as the background fluorescence could compromise our ability to clearly resolve signals associated with the influx of Ca^{2+}. (In contrast to previous reports (Issa and Hudspeth, 1994, 1996b), dense bodies were often not stained, and synaptic zones could be revealed only by Ca^{2+} influx. Only after repeated stimulation and Ca^{2+} current activation did the bodies gradually become stained.) We also sought active zones located toward the cell's cuticular plate. Because most active zones are concentrated toward the cell's basal pole, those located near the cuticular plate are relatively isolated and are less subject to fluorescence contributions due to signals originating in neighboring active zones (Roberts et al., 1990). Furthermore, in an effort to further reduce extraneous contributions, we used a near-minimum confocal aperture (~0.75 mm). Although this allowed us to study well-isolated active zones, it also limited the number of photons that we were able to collect from our area of interest. Thus despite a high photomultiplier gain, our signals rarely engaged the full 8-bit resolution of the confocal microscope. Confocal images obtained in this fashion have not been forced to comply to an 8-bit scale, and are displayed either in grayscale with arbitrary contrast or as pseudocolor images. Typically, after the entire cell was thoroughly scanned during depolarizing pulses, an isolated active zone was identified and then further examined by using the line scan mode of the microscope. Under these circumstances, the microscope repeatedly scans a particular transect of the cell, from left to right. Therefore one sacrifices spatial information (obtained by scanning different regions of a cell, as in Fig. 2 *A*) in exchange for the temporal resolution available when a single transect is scanned.

Diffusion-reaction modeling

To model the dynamics of Ca^{2+} entering the hair cell, we considered the problem as a diffusion reaction of Ca^{2+} from a single point source that represented the population of voltage-dependent Ca^{2+} channels present at a typical *R. pipiens* active zone. Here, at least three species would diffuse and react concurrently: Ca^{2+}, a Ca^{2+} buffer, and a Ca-buffer complex. For modeling purposes we subdivided the intracellular space into a cubic grid of unit "cells." The cubic grid went 60 layers deep into the hair cell. Each layer consisted of a plane of 30 cells × 30 cells, the side of each cubic cell being 140 nm long for modeling of fluorescence responses, and 10 nm long for modeling of Ca^{2+} profiles near the active zone (Fig. 5 *B*).

TABLE 1 Values and references for the parameters used in the model

Time step for model	2.0×10^{-4} s (except for Fig. 5B)
Width of model unit cell	140×10^{-9} m
Initial and background (boundary) Ca^{2+} concentration in the hair cell	$\sim 10^{-9}$ M*
Diffusion coefficient for Ca^{2+} in cytoplasm	600 $\mu m^2\ s^{-1}$
Initial and background (boundary) fluo-3 concentration in the hair cell	130 μM*
Diffusion coefficient for fluo-3 in cytoplasm (with or without bound Ca^{2+})	180 $\mu m^2\ s^{-1}$#
Dissociation constant of Ca · fluo-3	1 μM§
ON rate for Ca · fluo-3	$1.38 \times 10^9\ M^{-1}\ s^{-1}$¶
Endogenous Ca^{2+} buffer concentration in the hair cell	1 mM‖
Diffusion coefficient for endogenous Ca^{2+} buffer in cytoplasm (with or without bound Ca^{2+})	75 $\mu m^2\ s^{-1}$**
Dissociation constant of Ca · endogenous Ca^{2+} buffer	1 nM##
ON rate for Ca · endogenous Ca^{2+} buffer	$9.0 \times 10^7\ M^{-1}\ s^{-1}$##

*Estimated free Ca^{2+} and fluo-3 in whole-cell pipette
#Fig. 1 *C*.
§Fig. 1 *A*.
¶Eberhard and Erne (1989).
‖A plausible value, suggested by Roberts (1994).
**Fig. 1 *D*.
##Gross et al. (1993).

The binding of Ca^{2+} with a buffer (i.e., fluo-3 or an endogenous Ca^{2+} buffer) to form a Ca·buffer complex is described by

$$\text{Calcium(Ca)} + \text{Buffer}(B) \underset{K_{off}}{\overset{K_{on}}{\rightleftarrows}} \text{Complex}(\text{Ca} \cdot B)$$

K_{on} is the on rate of calcium binding to its buffer and K_{off} is the off rate of calcium from the Ca·buffer complex. As it pertains to endogenous buffers, this is a simplification, for a Ca^{2+}-binding molecule such as calbindin-D28k has four to six Ca^{2+}-binding sites. Thus, for a rigorous solution we would have to keep track of multiple species, an approach that was beyond our computational resources. To simplify matters, we considered only the high-affinity ($K_d \approx 10^{-9}$ M) Ca^{2+}-binding site and ignored the lower-affinity ones ($K_d \approx 10^{-5}$ M) (Gross et al., 1993).

Initial conditions for each cell were set with all diffusible species in equilibrium. The cell at the membrane surface, which surrounded the point source, was allowed to integrate the incoming current and develop an elevated Ca^{2+} concentration. Because *R. pipiens* saccular hair cells have 19 active zones, the value for the incoming Ca^{2+} current through the point source was set equal to 1/19 the experimentally measured Ca^{2+} current for each time step (Roberts et al., 1990). The concentration in the source cell due to the integrated current was given by

$$\text{Ca}_{\text{input}} = \frac{I_{\text{Ca}}}{4\pi \times F \times D_{\text{Ca}} \times L} + \text{Ca}_0 \qquad (1)$$

where I_{Ca} = 1/19 of the peak of the experimentally obtained input current, D_{Ca} is the diffusion coefficient of Ca^{2+}, F is the Faraday's constant, and L is the resolution of the cubic grid.

The three-dimensional diffusion and reaction of the three species was described in the following manner:

$$\frac{\partial \text{Ca}}{\partial t} = D_{\text{Ca}} \times \left(\frac{\partial^2 \text{Ca}}{\partial x^2} + \frac{\partial^2 \text{Ca}}{\partial y^2} + \frac{\partial^2 \text{Ca}}{\partial z^2}\right) - K_{\text{on}} \times B \times \text{Ca} + K_{\text{off}} \times (\text{Ca} \cdot B) \qquad (2)$$

$$\frac{\partial B}{\partial t} = D_{\text{B}} \times \left(\frac{\partial^2 B}{\partial x^2} + \frac{\partial^2 B}{\partial y^2} + \frac{\partial^2 B}{\partial z^2}\right) - K_{\text{on}} \times B \times \text{Ca} + K_{\text{off}} \times (\text{Ca} \cdot B) \qquad (3)$$

$$\frac{\partial (\text{Ca} \cdot B)}{\partial t} = D_{(\text{Ca}\cdot\text{B})} \times \left(\frac{\partial^2 (\text{Ca} \cdot B)}{\partial x^2} + \frac{\partial^2 (\text{Ca} \cdot B)}{\partial y^2} + \frac{\partial^2 (\text{Ca} \cdot B)}{\partial z^2}\right) + K_{\text{on}} \times B \times \text{Ca} - K_{\text{off}} \times (\text{Ca} \cdot B) \qquad (4)$$

Here Ca, B, and (Ca·B) are the absolute concentrations of Ca^{2+}, a buffer, and a Ca·buffer complex, respectively. To model results obtained with the inclusion of an endogenous Ca^{2+} buffer, an equation describing the diffusion reaction of Ca^{2+} with such a buffer was added, and the expressions above were appropriately modified. Although the model could also easily be modified to include a Ca^{2+} extrusion term, we decided not to incorporate this aspect of the ion's regulation. There are three reasons for this choice. First, for an ATP-dependent extrusion mechanism to counter the effects of Ca^{2+} entry near active zones, it would have to be packed into the nearby membrane at an extraordinarily high density (Roberts, 1994). No evidence for such specialization exists. Second, in some instances ATP was added to internal solutions before treatment with Chelex. In such cases the lack of Mg^{2+} would render the ATP ineffective as an energy source, yet we observed no detectable differences in fluorescence patterns. Third, studies in turtle hair cells indicate that the time constant for Ca^{2+} extrusion (10 s) is too slow to significantly affect the processes studied here (Tucker and Fettiplace, 1995).

For rapid convergence of the simultaneous equations, we used the Crank-Nicolson implicit method (Crank, 1975) concurrently with the successive overrelaxation (SOR) method (Smith, 1978). The Crank-Nicolson implicit iterative method consists of discretizing space, by creating cells, using the central difference method. Here we made no assumptions regarding the existence of a steady state at any particular time or place in the cell. This is essential for determining the distribution of the different reacting and diffusing species throughout the cell, particularly in the presence of large (50 pA) Ca^{2+} currents at individual active zones.

To compare experimentally obtained patterns of fluorescence with the predictions of the model, we assumed fluorescence to be directly proportional to the concentration of (Ca·B). At every iteration the results of the model were convolved with the point spread function for our confocal microscope, producing a pseudo-confocal image. We then scaled computed responses for 40-mV depolarizations to match the peak fluorescence experimentally obtained at this potential. The same scaling factor was then used to scale the calculated responses obtained at other potentials.

RESULTS

Because the theoretical model is only as accurate as the parameter values it employs, we worked to improve current estimates for a number of the model's parameters in hair cells. Our results suggest that often used estimates of important parameters are in considerable error.

Ca^{2+} affinity of fluo-3

To determine if the ionic form of fluo-3 trapped in hair cells behaves in a manner similar to that of the ionic form in free solution, we performed a [Ca^{2+}] versus fluo-3 fluorescence calibration curve for a cell loaded with fluo-3 AM. We exposed the indicator-loaded cell to increasing concentrations of extracellular Ca^{2+}, in the presence of 30 μg/ml of the Ca^{2+} ionophore A23187. Fig. 1 *A* shows the results obtained and compares them with those obtained in free solution by conventional fluorimetry (Fig. 1 *B*). Both curves yield a K_d for the Ca·fluo-3 complex of ~1 μM. This value agrees well with the published values of 0.4–0.55 μM (Eberhard and Erne, 1989; Issa and Hudspeth, 1996a). The correspondence between these two data sets suggests that the equilibrium behavior of the indicator inside intact cells and, for that matter, in those hair cells where the indicator was introduced through the whole-cell electrode, is comparable to that observed in free solution.

Diffusion coefficients and intracellular concentrations

We measured the diffusion coefficient for fluo-3 in fluo-3-AM-loaded cells by whole-cell recording. The diffusion coefficient for fluo-3 was estimated from the rate at which the indicator was lost from cells after break-in (Fig. 1 *C*). To ensure that the kinetics of fluo-3 fluorescence loss reflected the exit of indicator (rather than the rapid loss of Ca^{2+} from the cell), we dialyzed the cells with electrodes filled with an internal solution containing 10^{-7} M Ca^{2+}, a concentration comparable to that estimated for AM-loaded hair cells at rest. As shown below, the loss of fluorescence was well fitted by a single exponential, suggesting that a single process, namely the loss of indicator, is responsible for the time course of fluo-3 fluorescence decline.

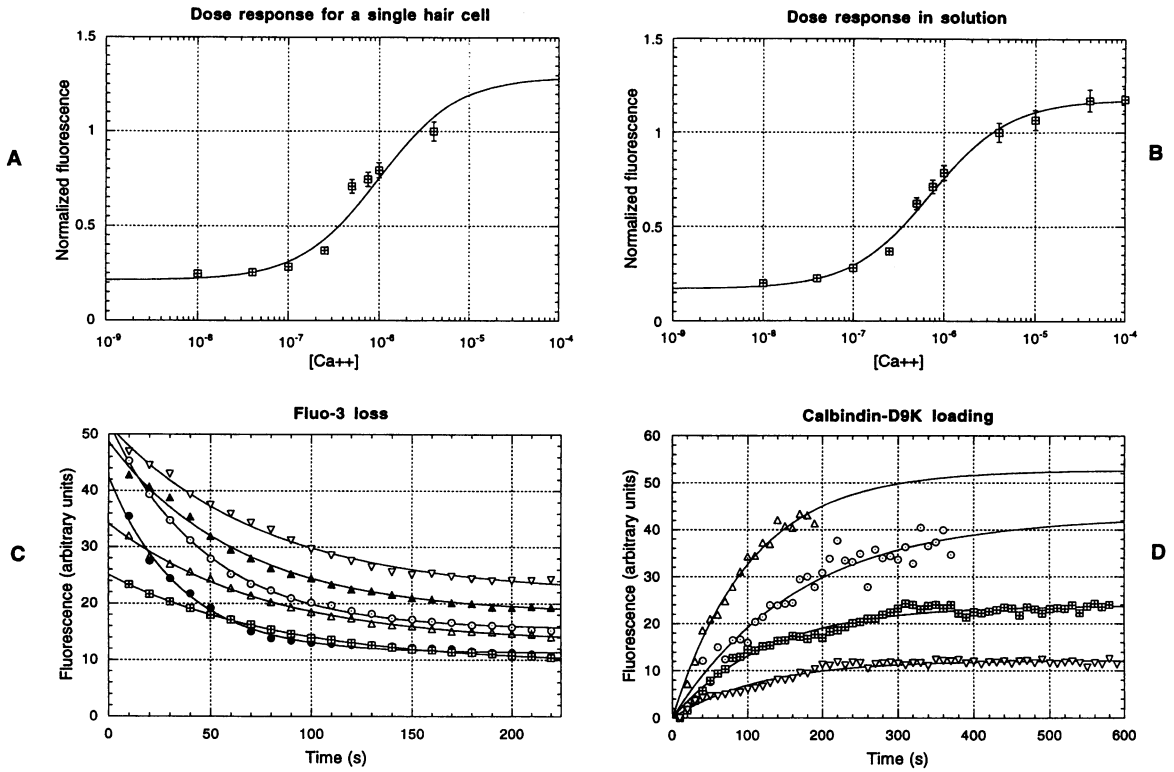

FIGURE 1 Measurement of parameter values for use in the model. (*A*) $[Ca^{2+}]$ versus fluo-3 fluorescence for a single hair cell. A hair cell was loaded with the cell-permeant form of fluo-3, and Ca^{2+} was admitted into the cell by the ionophore A23187. Full hair cell images were acquired and average fluorescence was determined from a region of the cell. (*B*) $[Ca^{2+}]$ versus fluo-3 fluorescence in free solution. Fluorescence in free solution was obtained by conventional spectrofluorimetry. Error bars in *A* and *B* represent the standard deviation of 24 and 100 time points, respectively. The data were normalized to the fluorescence at 4 μM Ca^{2+}. Fluorescence (F) dose-response curves were fitted according to $[Ca^{2+}] = K_d(f - f')/(1 - f)$, where $f = F/F_{maximum}$ and $f' = F_{minimum}/F_{maximum}$. (*C*) Diffusion of fluo-3 out of a hair cell. Six hair cells were loaded with the cell-permeant form of fluo-3. Tight seals were obtained with a patch pipette filled with an internal solution devoid of fluo-3. Full cell images were acquired every 10 s, and average fluorescence was determined from a representative region of the cell (the kinetics of exchange for both fluo-3 and calbindin-D9k were independent of the region chosen). Only fluorescence after break-in is plotted. Photobleaching of fluorescence was negligible, as estimated from neighboring cells. The loss of the cells' fluorescence is well fitted by the plotted single exponentials (data were fitted to $F = F_1 + F_2 \cdot e^{-t/\tau}$, where F_1 represents the fluorescence that remains trapped in the cell and F_2 represents the fluorescence that is lost through dialysis). The diffusion coefficient for fluo-3 is estimated at 176 ± 22 $\mu m^2\ s^{-1}$ according to Eq. 5. (*D*) Diffusion of calbindin-D9k into four different hair cells. Recording pipettes were filled with internal solution supplemented with ~1 mg/ml FITC · calbindin-D9k. Loading of the cell with the protein, after break-in, was monitored with full hair cell images acquired every 10 s. The increase in fluorescence was well fitted to $F = F_{max} \cdot (1 - e^{-t/\tau})$. The diffusion coefficient for calbindin-D9k is estimated at 103 ± 35 $\mu m^2\ s^{-1}$ according to Eq. 5.

The rate at which indicator is lost from the cytoplasm is related to its diffusion coefficient according to

$$D = \frac{R_s \cdot V}{\tau \cdot \rho} \tag{5}$$

where R_s is the series resistance (measured experimentally), V is the cell's volume (estimated from confocal images), τ is the time constant for indicator loss (estimated from single exponential fits), and ρ is the resistivity of the pipette's tip (Pusch and Neher, 1988; Marty and Neher, 1995). Tip resistivity was estimated for every cell as (series resistance/electrode resistance) × ρ', where ρ' is the experimentally determined resistivity of the pipette solution (69 Ω cm).

The estimated diffusion coefficient for fluo-3 is 176 ± 22 $\mu m^2\ s^{-1}$ (n = 6). This value is in good agreement with estimates for fura-2 in axons (211 $\mu m^2\ s^{-1}$ (Strautman et al., 1990)) and for fura-2 and calcium green in *Aplysia* neurons (132 $\mu m^2\ s^{-1}$; Gabso et al., 1997).

Calcium-binding proteins have been proposed to play a role in buffering Ca^{2+} in hair cells. Although calmodulin and calbindin-D28k have been shown to be present in amphibian hair cells (Sheperd et al., 1989), other proteins are also considered as possible candidates for a buffering role. These include α-parvalbumin, calretinin, and oncomodulin. To obtain an estimate for the diffusion of globular Ca^{2+}-binding proteins in hair cells, we used the readily available calbindin-D9K. The diffusion coefficient for this molecule was obtained from the rate at which the FITC-labeled protein loaded into hair cells after break-in. The estimated value, 103 ± 35 $\mu m^2\ s^{-1}$ (n = 4), is comparable to estimates for diffusion in water of proteins of comparable size (Popov and Poo, 1992). If we assume that $D \propto (MW)^{1/3}$ (Pusch and Neher, 1988), then the diffusion coefficient for

a molecule the size of calbindin-D28k can be estimated as $103 \times (11\ kDa/28\ kDa)^{1/3}$, that is 75 $\mu m^2\ s^{-1}$. Note that we use here the effective molecular weight for calbindin-D9k as determined by gel filtration.

Fluorescence versus Ca^{2+} current under whole-cell recording conditions

Focal entry of Ca^{2+} can be visualized with the use of Ca^{2+}-sensitive indicators (Issa and Hudspeth, 1994, 1996b). An example of this localized signal is shown in Fig. 2. This cell was voltage-clamped using the conventional whole-cell recording technique with a pipette containing 130 μM fluo-3. Note the barely noticeable fluorescent dense bodies (*white asterisks*), which are indicators of the synaptic active zones (Fig. 2 *A*). Fig. 2 *B* shows the average of six such images with depolarizations that elicited large Ca^{2+} currents (150-ms depolarizations, each of 40, 60, or 80 mV). Of the several active zones in this focal plane, only one (*arrow*) was scanned while the cell was being depolarized, and therefore it shows the maximum increase in fluorescence. Active zones situated to the left of the horizontal bar that represents the depolarizing step show no increase in fluorescence because they were scanned before the cell is depolarized, whereas those situated to the right of the stimulus bar failed to show an increase in fluorescence because of the rapid closure of Ca^{2+} channels after the termination of the pulse (a similar effect is shown in Fig. 4 *A*). This lack of temporal resolution can be avoided (at the expense of spatial information) by the use of line scanning.

After identification of an isolated active zone, line scanning (2 ms/line) was performed while the depolarization

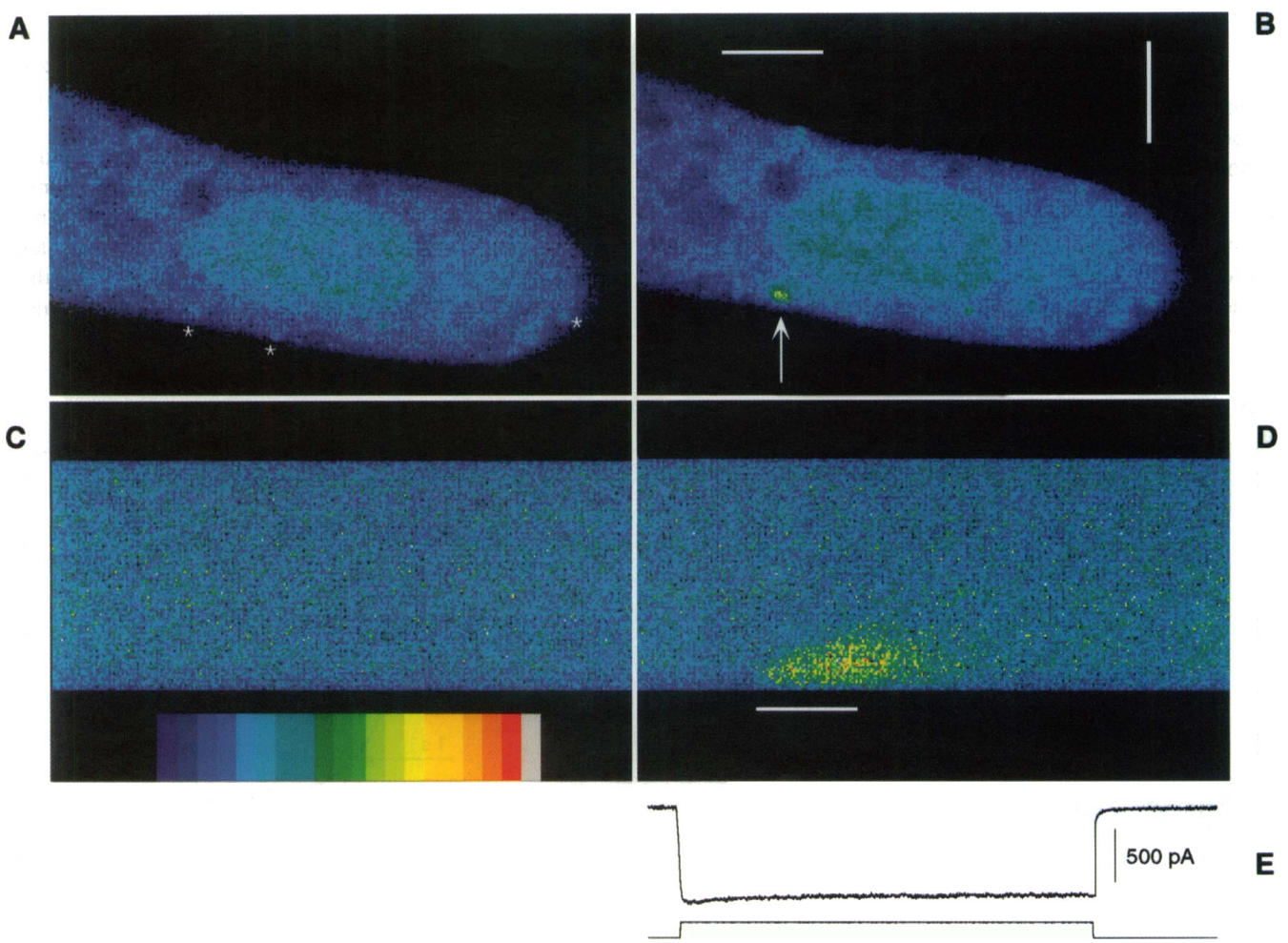

FIGURE 2 Ca^{2+}-induced fluo-3 fluorescence under whole-cell recording conditions. (*A*) Average of four images. Two images were acquired while the cell was maintained at a holding potential of −65 mV, and two were acquired during 20-mV depolarizations that did not elicit Ca^{2+} currents. (*B*) Average of six images. Two images, each acquired during depolarizations of 40, 60, and 80 mV, which elicited large Ca^{2+} currents. To remove fluorescence noise in *A* and *B*, we averaged images of this cell obtained under similar circumstances and within seconds of each other. All averaged images had a similar appearance, i.e., no single image biased the average. (*C*) Line scan fluo-3 fluorescence from a different cell held at −65 mV. (*D*) Line scan fluo-3 fluorescence during a 40-mV depolarization (no averaging in line scans). Note the rapid increase in fluorescence after pulse onset, the deep spatial penetration into the cell, and the slow decay after termination of the pulse. Vertical scale bar = 5 μm. Horizontal scale bars = 150 ms depolarization. Color scale = 0–63 arbitrary fluorescence units. (*E*) Whole-cell current elicited by the 40-mV depolarizing protocol. Capacitative current artifacts (1.0 ms) were digitally removed.

stimulus was repeated. The depolarizing pulses elicited robust voltage-dependent Ca^{2+} currents ranging from ~60 pA to nearly 1 nA (data not shown). The resulting increase in fluo-3 fluorescence paralleled the amplitude of the Ca^{2+} currents. The depolarization that elicited the largest peak Ca^{2+} current also elicited the most intense and deeply penetrating fluo-3 fluorescence (Fig. 2, *D–E*). The signal extended well beyond the limits of the dense body (~400 nm). Therefore, this change in fluo-3 fluorescence reflects a change in cytoplasmic Ca^{2+} rather than a change restricted to the dense body. Ca·fluo-3 fluorescence increased monotonically during the stimulus, and then returned to baseline with a time course that was well fitted by the sum of two exponentials (Fig. 3 *B*): a dominant (70%) 115-ms component and a minor slow one with a time constant of ~1.5 s. In every case where we were able to induce a significant Ca^{2+} current (>100 pA), we observed a clear increase in fluorescence (at least 14 cells from six animals) and a relatively persistent component of fluorescence.

Modeling the space, time, and voltage dependence of Ca^{2+}-induced fluorescence under whole-cell conditions

We then addressed whether the spatial and temporal aspects of the fluorescence signals obtained at different potentials could be explained by a relatively simple diffusion-reaction model. The model examined the diffusion of Ca^{2+}, fluo-3, and the Ca·fluo-3 complex, as well as the chemical binding reaction between these species.

Based on Eq. 5, and considering our estimates for diffusion coefficients as well as the time elapsed after break-in at which recordings were performed, it is reasonable to assume that the intracellular concentrations of Ca^{2+} and fluo-3 are equal to the concentrations present in the recording pipette (Table 1). The model was driven by the expected influx of Ca^{2+} at an active zone, given the cell's experimentally recorded Ca^{2+} current (Fig. 2 *E*). Three points are pertinent regarding the use of these currents to drive the model. First, these voltage-dependent inward currents are carried by Ca^{2+}, i.e., there are no voltage-dependent Na^{+} channels in these hair cells. Second, Ca^{2+} channels in the frog's vestibular hair cells do not inactivate. Therefore, the decline in peak Ca^{2+} current visible at some potentials is due to a residual K_{Ca} outward current that is not blocked by cesium (Hudspeth and Lewis, 1988). Third, because the typical *R. pipiens* saccular hair cell possesses 19 ± 2 active zones, the amplitude of the Ca^{2+} current at the modeled active zone was assumed to be 1/19 of the total peak current (Roberts et al., 1990).

The simple diffusion-reaction model predicts a rapid increase in Ca·fluo-3 fluorescence after a depolarization onset, and a deep penetration of free Ca^{2+} into the cell. These results agree reasonably well with those experimentally determined (compare Fig. 3 *A*, *bottom* and *middle*). Furthermore, when the same scaling factor was applied, the mod-

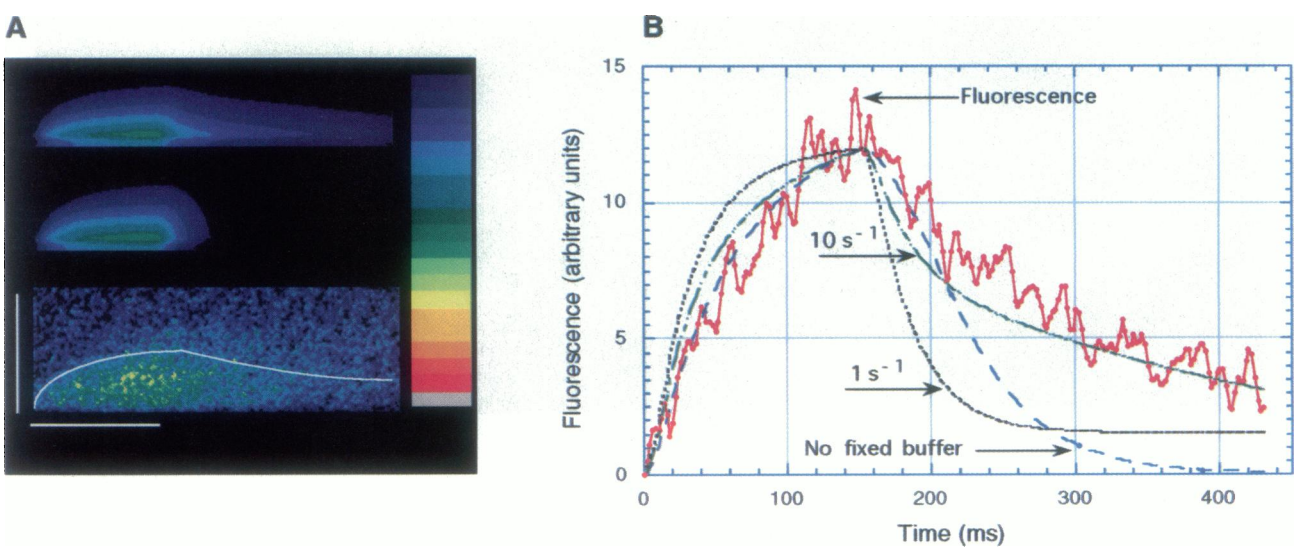

FIGURE 3 Modeling Ca^{2+} · fluo-3 fluorescence patterns in hair cells. (*A*) *Bottom*: Line-scan data from Fig. 2 *D*, 40-mV depolarization. Background fluorescence has been subtracted, leaving, in addition to the signal, random fluctuations in fluorescence intensity. *Middle*: Pseudo-confocal line-scan image of data generated by the model, considering only Ca^{2+} and fluo-3 as active species in the cell. *Top*: Pseudo-confocal line-scan image of data generated by the model considering Ca^{2+}, fluo-3, and 200 μM of a fixed Ca^{2+} buffer. The peak concentrations generated by the model (*middle* and *top*) have been scaled, independently, to comply with the fluorescence scale from the experimental data (*bottom*). Vertical scale bar = 5 μm. Horizontal scale bar = 150-ms depolarization. Color scale = 0–47 arbitrary fluorescence units. For comparison, the outline of the response obtained with a fixed buffer (*top*) has been superimposed on the line scan image. (*B*) Effect of the off-rate of a fixed buffer on the predicted patterns of fluorescence. Average fluorescence up to 5 μm away from the membrane is plotted as a function of time. Because of the deep penetration of the signal, these averages do not represent a distorted value, and similar plots were obtained when fluorescence in the vicinity of the membrane (1 μm) was plotted. The model included 200 μM fixed Ca^{2+} buffer, with varying affinities (off rates) for Ca^{2+}. Plots were individually scaled to match the observed peak fluorescence.

el's predictions for 20-, 60-, and 80-mV depolarizations produced a similar agreement (data not shown). Although the results of the simple diffusion-reaction model generally resemble those obtained experimentally, the model fails in its prediction of the decay time of the fluorescent signal after the termination of the voltage pulse. Whereas the experimentally observed fluorescence decays slowly, the simple diffusion-reaction model predicts a very rapid decay (Fig. 3 *B*). No realistic combination of model parameters could accurately account for the observed decay of Ca^{2+}-induced fluorescence.

The model's failure in this area forced us to consider the possibility that some of the hair cell's endogenous Ca^{2+} buffers might have been retained by the cell, despite the fact that the confocal data were typically collected a few to several minutes after break-in. For example, the images presented in Fig. 2 were obtained ~4 min after break-in to establish the whole-cell recording configuration. However, 4 min is not sufficient for the complete exchange of even a small Ca^{2+}-binding protein (Fig. 1 *D*) (relatively rapid washout of Ca^{2+} currents prevented us from waiting for a more complete dialysis of cellular contents). If a cell contains 1 mM calbindin-D28k, 4 min after break-in the cell would still retain a concentration of protein of several hundred μM. Inclusion of 300 μM of a mobile Ca^{2+} buffer did not change the model's results sufficiently to explain the persistence of Ca·fluo-3 fluorescence after the termination of the pulse. Such a failure can be explained by the slow rate at which the buffer releases Ca^{2+} (0.09 s^{-1}), combined with the effectiveness with which such a highly mobile buffer is cleared from the synaptic area.

The persistence of fluorescence can, however, be predicted by including a very slowly diffusing, or even immobile, Ca^{2+} buffer in the model (Fig. 3 *A*, *top*). To explain a slow component of fluorescence decay, one can assume an off rate of ~10 s^{-1} for this fixed buffer. The buffer binds Ca^{2+} during the pulse and then slowly releases it after the termination of the pulse. As Ca^{2+} is released it can rebind to fluo-3, thus extending the lifetime of the fluorescent signal. Altering the off rate of the buffer has a substantial effect on the time course of the signal's persistence (Fig. 3 *B*). A fixed buffer of lower affinity ($K_d > 10^{-6}$ M) is of no consequence for the decay of fluorescence, for it releases its bound Ca^{2+} nearly instantly. Conversely, a higher-affinity buffer ($K_d < 10^{-7}$ M) retains it for far too long.

Fluorescence versus Ca^{2+} current under perforated-patch recording conditions

Data obtained under whole-cell recording conditions are affected by the fact that the internal milieu of the cell has been altered. To preserve the intracellular contents, we used the perforated-patch recording technique (Horn and Marty, 1988). Fluorescence data obtained with the perforated-patch method differed from whole-cell data in two ways. First, the fluorescent signal appeared to be more sharply focused than under whole-cell conditions, barely spreading beyond the edges of the lightly stained dense bodies (Fig. 4 *B*). Second, fluorescent signals were quite weak, despite the presence of robust (>1 nA) Ca^{2+} currents. The interpretation of full hair cell images was confirmed when line scans were acquired of perforated-patch clamped hair cells (Figs. 4, *C* and *D*). Line scans revealed a pattern of fluorescence that again was lower in intensity and more confined to the immediate vicinity of the cell membrane than that observed under whole-cell clamp conditions. However, the time course of the rise and fall of fluorescence was roughly similar to that observed under whole-cell conditions (Fig. 3 *B*) (not shown).

The spatial profile of fluo-3 fluorescence is shown in Fig. 5 *A*, by plotting the average fluo-3 fluorescence during the last 20 ms of the depolarizing pulse. Unavoidably, this is a noisy signal because we are plotting fluorescence values in different regions of a nonhomogeneous cell. However, it is clear that the model predicts a relatively narrow peak of fluorescence, even in the absence of endogenous buffer, whereas the experimentally observed fluorescence pattern obtained under whole-cell recording conditions is relatively broad. Note that plotting the normalized model results underemphasizes the differences arising from the inclusion of buffer in the model. The peak calculated Ca^{2+}-induced fluorescence in the presence of the buffer is ~20% that obtained in the absence of buffer. Model calculations (not shown) indicate that for large currents, fluo-3 is severely depleted near the membrane, limiting the indicator's ability to faithfully report changes in Ca^{2+} concentration. Furthermore, although the recording pipette is practically an infinite reservoir of indicator, its bandwidth is limited, as implied by Eq. 5. Therefore, to assume that the concentration of indicator at the boundaries of the modeled space is equal to that present in the pipette might not be entirely justified. A pattern of fluorescence with a relatively narrow peak near the membrane was observed under perforated-patch recordings (Fig. 5 *A*). This might be due, in part, to endogenous mobile Ca^{2+} buffer capture of incoming Ca^{2+}, thus limiting the depletion of Ca^{2+}-free fluo-3 near the membrane.

The restricted spread of fluo-3 fluorescence observed with peforated patch recordings (compare Figs. 2 and 4) cannot be explained by indicator compartmentalization into membrane-bounded organelles. As Fig. 1 shows, only about one-third of the indicator is immobilized. Furthermore, rather than being compartmentalized into membranous organelles, this indicator is simply immobilized. Simplest to interpret is the fact that the fraction of immobilized indicator in the hair bundle, a region evidently lacking membrane-bound organelles, is the same as in the rest of the cell. In some instances repeated scanning of a cell region led to an irreversible increase in fluorescence in that region, suggesting the possibility that indicator may be immobilized by photo-cross-linking to intracellular elements (not shown). Immobilized indicator, therefore, simply adds a mildly elevated fluorescence background. Furthermore, this restricted

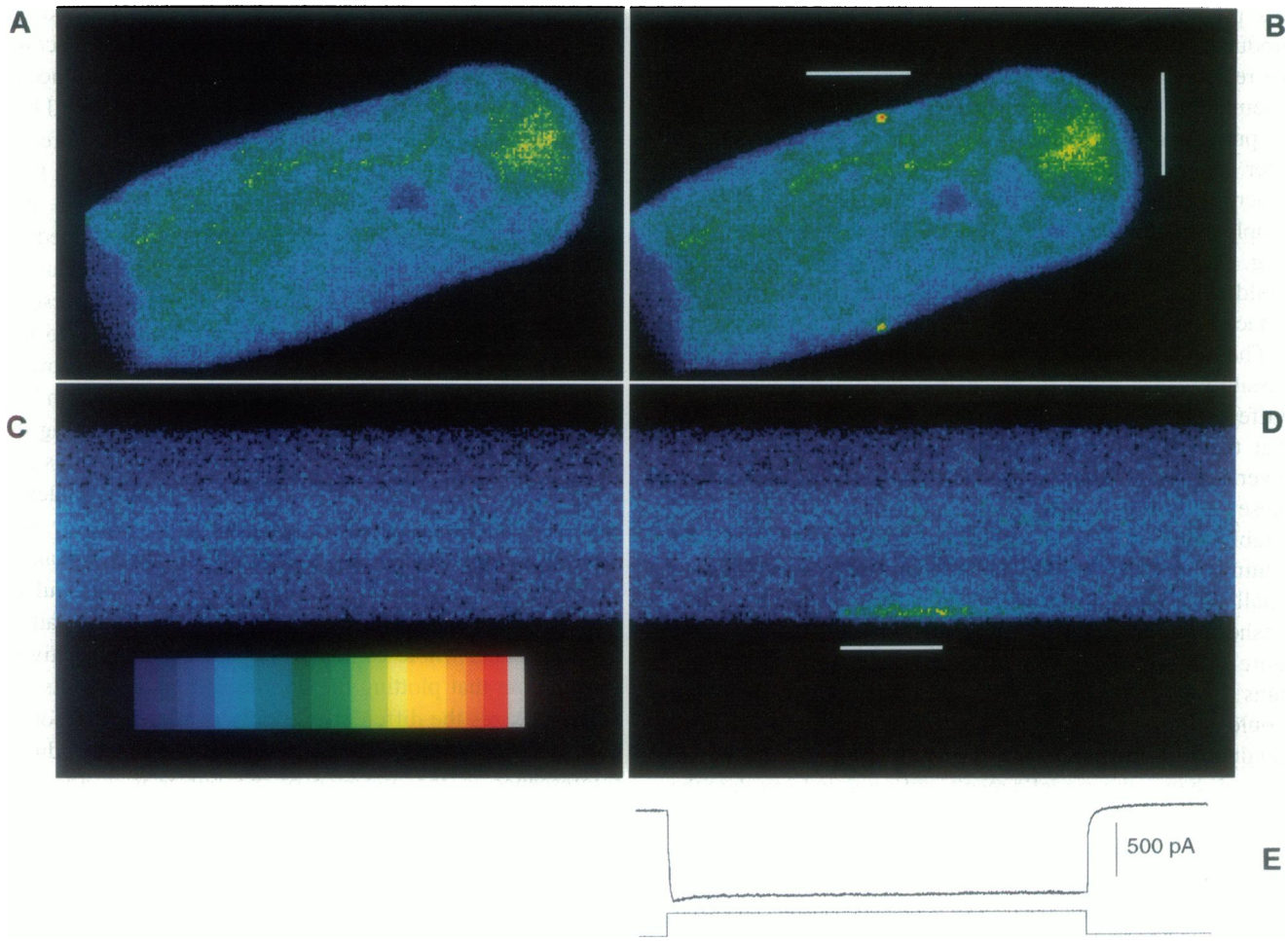

FIGURE 4 Ca^{2+}-induced fluo-3 fluorescence under perforated-patch recording conditions. (*A*, *B*, and *C*) As in Fig. 2. Note the sharply defined Ca^{2+} microdomains shown in *B*. (*D*) Line-scan fluo-3 fluorescence during a 60-mV depolarization. Note the restricted penetration of Ca^{2+}-induced fluorescence into the cell, and the slow decay after termination of the pulse. Vertical scale bar = 5 μm. Horizontal scale bars = 150 ms depolarization. Color scale = 0–63 arbitrary fluorescence units. (*E*) Whole-cell currents elicited by the depolarizing protocol. Capacitative current artifacts (0.5 ms) were digitally removed.

spread of fluo-3 fluorescence also cannot be explained by an excessively large amount of indicator trapped in the cell acting as a mobile Ca^{2+} buffer. We estimated the concentration of fluo-3 under perforated patch by comparing $F_{minimum}$ under whole-cell conditions ([Ca] $<$ 1 nM) with that observed for AM-loaded cells exposed to Ca^{2+} ionophore and to very low extracellular Ca^{2+} concentrations (10 nM). These two values were quite similar, indicating that the concentration of indicator under perforated patch conditions is $\sim$115 μM.

The dynamics of Ca^{2+} at the active zone

Fluorescent signals have a lateral resolution of $\sim$0.5 μm, a size roughly comparable to the dimensions of the hair cell's active zone. Thus it is clear that they cannot give us information about the dynamics of Ca^{2+} near transmitter release sites, an issue of central importance to our understanding of synaptic transmission. However, to the extent that our model provides a reasonable account of fluorescent responses, we feel confident enough about its use to explore the dynamics of Ca^{2+} at the submicrometer level. To this effect we solved the model for an idealized active zone (Fig. 5 *B*), consisting of an array of 85 Ca^{2+} channels (Roberts, 1994). The model was driven by the Ca^{2+} current expected for a 25-mV, 1-kHz sinusoidal depolarization (Hudspeth and Lewis, 1988; Colquhoun and Hawkes, 1995). The inclusion of a mobile buffer in the model causes a more rapid reestablishment of the background Ca^{2+} concentration after a depolarizing half-cycle. A similar effect can also be observed at 100 Hz, a frequency more relevant to the physiology of vestibular hair cells. At this lower frequency there is more time for recovery between successive periods of depolarization. However, this gain is offset by larger Ca^{2+} entry, as a consequence of longer and more complete Ca^{2+} channel activation.

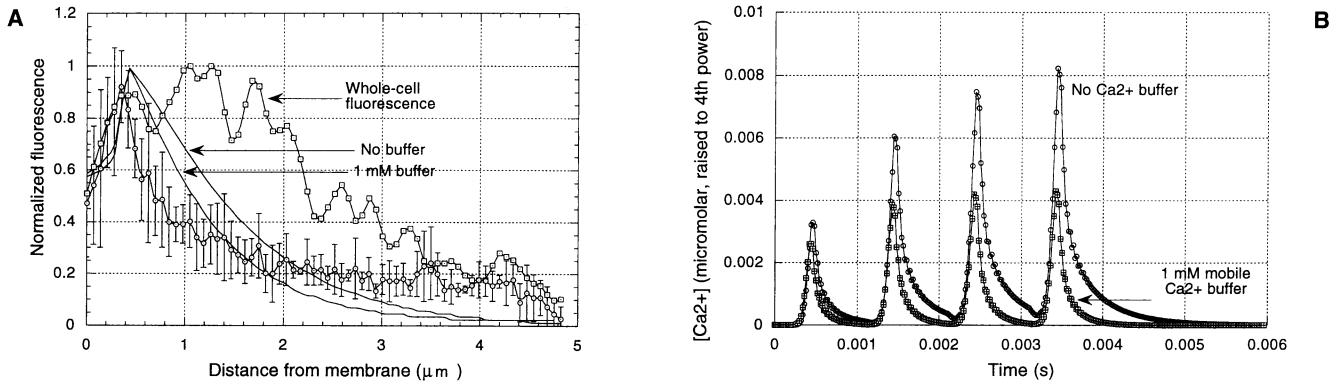

FIGURE 5 Modeling the effects of an endogenous Ca^{2+} buffer. (*A*) Spatial profile of fluo-3 fluorescence under whole-cell and perforated-patch conditions. The average fluorescence during the last 20 ms of the depolarizing pulse is plotted against distance from the membrane. Values for perforated-patch conditions are the average of four cells, ± SD. For comparison, average fluorescence was normalized to the individual cells' peak value. Model solutions were obtained with and without 1 mM endogenous mobile buffer. (*B*) Effect of endogenous buffer on the Ca^{2+} concentration near active zones. Ca^{2+} channel gating was modeled according to a previously published gating scheme, by allowing pseudo-random gate transitions. The holding potential was set at −70 mV, and the stimulus was a sinusoidal, 25-mV (peak), 1000-Hz depolarizing train (peak $P_{open} \approx 0.01$). Ca^{2+} channel gating was modeled with a 1-μs step, and the diffusion reaction model was run with a 20-μs step and a 10-nm cell size. The current associated with an open channel was set at 0.5 pA. The time-averaged, single-channel current was allowed to flow through all (85) channels in the active zone. Because of the steep dependence of transmitter release on $[Ca^{2+}]$, the fourth power of the concentration of Ca^{2+} at the geometrical center of the active zone is plotted.

DISCUSSION

Endogenous mobile buffers curb the spread of free calcium

Under perforated-patch conditions, Ca^{2+}-induced fluo-3 fluorescence is restricted to the immediate vicinity of the cell membrane (Figs. 4, *B* and *D*, and 5 *A*). The loss of endogenous mobile Ca^{2+} buffers after break-in allows Ca^{2+} to penetrate deeply into the cell (Fig. 2, *B* and *D*). Theoretical studies indicate that, unless it is buffered, free Ca^{2+} can propagate far beyond its intended site of action at the synapse (Roberts, 1994; Wu et al., 1996). Our observations provide the first direct evidence for this role of endogenous buffers in hair cells. Such highly localized Ca^{2+} signaling might be essential for the independent operation of neighboring efferent and afferent synapses, both of which employ Ca^{2+} as a second messenger (Jaramillo, 1995).

The simplest diffusion-reaction scheme is not sufficient to explain the observed patterns of Ca^{2+}-induced fluo-3 fluorescence

A persistent component of fluorescence after the termination of a stimulus required us to include 200 μM of a moderately high-affinity, fixed (or nearly immobile) buffer component. Fixed buffers are generally thought to comprise numerous molecular species, with varying abundance and kinetic parameters. There is little doubt that they are present in all cell types, and current evidence indicates that the majority of Ca^{2+} entering a cell is captured by these as well as by mobile buffers (Albritton et al., 1992; Al-Baldawi and Abercrombie, 1995). Although this choice appears reasonable to us, it is simply a guess, to be refined as information about these buffers in hair cells emerges.

This work follows the earlier work of Issa and Hudspeth on amphibian hair cells (Issa and Hudspeth, 1994, 1996a,b). Although their work makes significant theoretical points, it does not attempt to fully explain the spatial and temporal characteristics of Ca^{2+}-induced patterns of fluorescence. Our work represents the first attempt to reconcile in detail a diffusion reaction scheme with high-resolution fluorescence measurements in hair cells. We have undertaken this in the most thorough way we can, by seeking to reproduce the observed patterns of fluorescence (Fig. 3). Previously it has been claimed that a simple diffusion-reaction scheme can account for observed patterns of fluorescence (Issa and Hudspeth, 1996). However, the mentioned work focuses on the fluorescence at the synaptic dense bodies, rather than throughout the cell. Furthermore, the unrealistic values given to certain model parameters (i.e., $D_{fluo-3} = 40\ \mu m^2\ s^{-1}$) limits the validity of this claim. Our model provides, at best, a rough correspondence between expected and observed patterns of Ca^{2+}-induced fluorescence. A full description of these patterns will probably require the simultaneous inclusion in the model of Ca^{2+} and an indicator, as well as of fixed and mobile endogenous buffer species, a feat currently beyond our capabilities. Furthermore, it might be necessary to include the multiple binding affinities that define the properties of these endogenous buffers. Future work will be required to elucidate the identity of the actual species involved in Ca^{2+} buffering in hair cells.

Theoretical modeling predicts sharply defined Ca^{2+} microdomains (radius < 0.5 μm) near active zones. Such a prediction, originally confirmed by others (Issa and Hudspeth, 1994, 1996), is extended here by the use of the perforated-patch technique. However, other experimental studies reveal domains of elevated Ca^{2+} in turtle hair cells that are considerably broader than theoretically expected. These large domains might arise from the contribution of

several isolated microdomains, which remain unresolved as a consequence of the limited optical resolution afforded by low-numerical-aperture objectives and slit confocal microscopy (Tucker and Fettiplace, 1995).

Endogenous Ca^{2+} buffers in hair cells are highly mobile

Our results do not imply that calbindin-D9k plays a role in Ca^{2+} buffering in hair cells. However, the kinetics of calbindin-D9K exchange (Fig. 1 *D*) suggest that the diffusion coefficient for Ca^{2+}-binding proteins in hair cells is considerably higher than previously thought. For instance, our estimate for the diffusion coeficient for calbindin-D28k, 75 $\mu m^2\ s^{-1}$, is considerably higher than the commonly assumed value of 20 $\mu m^2\ s^{-1}$. This smaller value is based on estimates for diffusion of macromolecules in growth cones (Popov and Poo, 1992). However, such assumptions ignore the possibility that specific cellular constituents can significantly alter the diffusion of particular species. An example of such an effect can be found in the diffusion of Ca^{2+} indicators. Such diffusion is nearly unimpeded in axons or in large *Aplysia* neurons, yet is restricted in muscle cells (Baylor and Hollingworth, 1988; Strautman et al., 1990).

Fig. 5 *B* illustrates the effect of a mobile Ca^{2+} buffer in the dynamics of Ca^{2+} at the active zone. In the absence of mobile buffer, even a weak periodic stimulus leads to a gradual accumulation of Ca^{2+} at this site (a steady state is reached in a relatively small number of cycles). Such "residual" Ca^{2+} is thought to underlie time-dependent changes in synaptic strength such as facilitation. However, evidence indicates that hair cell synapses operate in a nearly history-independent fashion, even at frequencies as high as 10 kHz (Hind et al., 1966). The presence of mobile buffers could largely suppress this time-dependent Ca^{2+} accumulation.

The mobility of Ca^{2+} buffers is of little consequence for the behavior illustrated in Fig. 5 *B*, that is, results obtained with a buffer 1/10 as mobile are nearly indistinguishable from those shown. However, as Ca^{2+} accumulates, the endogenous buffer becomes severely depleted. Given a certain concentration of buffer in the cytoplasm, it is the buffer mobility that determines the cell's ability to replenish depleted buffer near the cell membrane (Roberts, 1994). Thus a high buffer mobility might be crucial during prolonged or saturating stimuli.

Drs. R. Abercrombie, P. Gillespie, and S. Treynelis kindly provided comments on the manuscript. We thank Drs. N. Issa and P. Becker for valuable discussions and Dr. C. Angeletti for help with microfluorimetry.

This work was supported by National Institute on Deafness and Other Communication Disorders grant DC02235. FJ is an Alfred P. Sloan Fellow.

REFERENCES

Al-Baldawi, N., and R. F. Abercrombie. 1995. Calcium diffusion coefficient in Myxicola axoplasm. *Cell Calcium.* 17:422–430.

Albritton, N. L., T. Meyer, and L. Stryer. 1992. Range of messenger action of calcium and inositol 1,4,5-trisphosphate. *Science.* 258:1812–1815.

Assad, J. A., N. Hacohen, and D. P. Corey. 1989. Voltage dependence of adaptation and active bundle movement in bullfrog saccular hair cells. *Proc. Natl. Acad. Sci. USA.* 86:2918–2922.

Baylor, S. M., and S. Hollingworth. 1988. Fura-2 calcium transients in frog skeletal muscle fibres. *J. Physiol. (Lond.).* 403:151–192.

Colquhoun, D., and A. G. Hawkes. 1995. The principles of the stochastic interpretation of ion-channel mechanisms. *In* Single-Channel Recording, 2nd ed. B. Sakmann and E. Neher, editors. Plenum Publishing, New York.

Crank, J. 1975. Mathematics of Diffusion. Clarendon Press, Oxford.

Eberhard, M., and P. Erne. 1989. Kinetics of calcium binding to fluo-3 determined by stopped-flow fluorescence. *Biochem. Biophys. Res. Commun.* 163:309–314.

Gasbo, M., E. Neher, and M. E. Spira. 1997. Low mobility of the Ca^{2+} buffers in axons of cultured Aplysia neurons. *Neuron.* 18:473–481.

Gross, M., A. Gosnell, A. Tsarbopoulos, and W. Hunziker. 1993. A functional and degenerate pair of EF hands contain the very high affinity calcium-binding sites of calbindin-D28k. *J. Biol. Chem.* 268: 20917–20922.

Hind, J. E., D. J. Anderson, J. F. Brugge, and J. E. Rose. 1966. Phase-locked response to low frequency tones in single auditory nerve fibers of the squirrel monkey. *J. Neurophysiol.* 30:769–793.

Horn, R., and A. Marty. 1988. Muscarinic activation of ionic currents measured by a new whole-cell recording method. *J. Gen. Physiol.* 92:145–159.

Hudspeth, A. J., and R. S. Lewis. 1988. Kinetic analysis of voltage- and ion-dependent conductances in saccular hair cells of the bull-frog, *Rana catesbeiana. J. Physiol. (Lond.).* 400:237–274.

Issa, N. P., and A. J. Hudspeth. 1994. Clustering of Ca^{2+} channels and Ca^{2+} -activated K^+ channels at fluorescently labeled presynaptic active zones of hair cells. *Proc. Natl. Acad. Sci. USA.* 91:7578–7582.

Issa, N. P., and A. J. Hudspeth. 1996a. Characterization of fluo-3 labelling of dense bodies at the hair cell's presynaptic zone. *J. Neurocytol.* 25:257–266.

Issa, N. P., and A. J. Hudspeth. 1996b. The entry and clearance of Ca^{2+} at individual presynaptic active zones of hair cells from the bullfrog's sacculus. *Proc. Natl. Acad. Sci. USA.* 93:9527–9532.

Jaramillo, F. 1995. Signal transduction in hair cells and its regulation by calcium. *Neuron.* 15:1227–1230.

Jaramillo, F., S. Betarbet, and J. D. Hall. 0000. Calcium transients in hair cells: mathematical modeling of confocal microscopy observations. *Soc. Neurosci. Abstr.* 423:11.

Marty, A., and E. Neher. 1995. Tight-seal whole-cell recording. *In* Single-Channel Recording, 2nd ed. B. Sakmann and E. Neher, editors. Plenum, New York.

Popov, S., and M. Poo. 1992. Diffusional transport of macromolecules in developing nerve processes. *J. Neurosci.* 12:77–85.

Pusch, M., and E. Neher. 1988. Rates of diffusional exchange between small cells and a measuring patch pipette. *Pflugers Arch.* 411:204–211.

Roberts, W. M. 1993. Spatial calcium buffering in hair cells. *Nature.* 363:74–76.

Roberts, W. M. 1994. Localization of calcium signals by a mobile calcium buffer in frog saccular hair cells. *J. Neurosci.* 14:3246–3262.

Roberts, W. M., R. A. Jacobs, and H. A. J.. 1990. Colocalization of ion channels involved in frequency selectivity and synaptic transmission at presynaptic active zones of hair cells. *J. Neurosci.* 10:3664–3684.

Schefer, U., D. Ammann, E. Pretsch, U. Oesch, and W. Simon. 1986. Neutral carrier based Ca^{2+}-selective electrode with detection limit in the sub-nanomolar range. *Anal. Chem.* 58:2282–2285.

Sheperd, G. M. G., B. A. Barres, and D. P. Corey. 1989. "Bundle blot" purification and initial protein characterization of hair cell stereocilia. *Proc. Natl. Acad. Sci. USA.* 86:4973–4977.

Smith, G. D. 1978. Numerical Solution of Partial Differential Equations. Clarendon Press, Oxford.

Strautman, A. F., R. J. Cork, and K. R. Robinson. 1990. The distribution of free calcium in transected spinal axons and its modulation by applied electrical fields. *J. Neurosci.* 10:3564–3575.

Tucker, T., and R. Fettiplace. 1995. Confocal imaging of calcium microdomains and calcium extrusion in turtle hair cells. *Neuron.* 15:1323–1335.

Wu, Y. C., T. Tucker, and R. Fettiplace. 1996. A theoretical study of calcium microdomains in turtle hair cells. *Biophys. J.* 71:2256–2275.